DALTON

Dihydroxotitanium(IV) phosphate: characterisation and studies of *n*-alkylamine intercalation, ion-exchange properties, and proton conduction

Enrique Jaimez and Robert C. T. Slade*

Department of Chemistry, University of Exeter, Stocker Road, Exeter EX4 4QD, UK

The thermal behaviour and porosity of the dihydroxotitanium(IV) phosphate $Ti(OH)_2(HPO_4)\cdot H_2O$ have been investigated. The intercalation of *n*-alkylamines, ion-exchange behaviour, and near-ambient-temperature proton conduction have also been studied and are discussed in comparison with the behaviour of layered crystalline titanium(IV) phosphates.

Many studies on the synthesis and characterisation of metal(IV) phosphates with lamellar structures have been reported; structural features, physicochemical properties and applications of this rapidly growing class have been the subject of a number of reviews.[1–4] Such compounds show a high stability against degradation and in suspension are cation exchangers.[5] Their property of intercalation of polar organic molecules, ionic conductivity and potential as catalysts are well known.[6–8] Layered titanium(IV) acid phosphates are usually synthesized from a preformed amorphous titanium phosphate, which is further treated with H_3PO_4(aq) either under reflux or hydrothermally. The crystalline compounds α-titanium phosphate [α-TiP, $Ti(HPO_4)_2\cdot H_2O$] and γ-titanium phosphate [γ-TiP, $Ti(H_2PO_4)(PO_4)\cdot 2H_2O$] are well characterised. Titanium phosphates can also be prepared as gels and in intermediate stages of crystallinity,[9] the product obtained depending on the working conditions.[10]

Recent papers reported the synthesis of two novel hydroxyphosphates of titanium(IV).[11,12] In this paper the chemistry of $Ti(OH)_2(HPO_4)\cdot H_2O$, Ti(OH)P, is further elaborated; the surface area and porosity, *n*-alkylamine intercalation chemistry, ion-exchange properties and proton conductivity have been investigated.

Results and Discussion

Characterisation

Fig. 1 shows both TG and DTA traces for a sample of Ti(OH)P stored over anhydrous $CaCl_2$(s). Dehydration takes place in three steps, the mass losses associated with the first two ($\Delta m \approx 18\%$ at 25–380 °C) being very similar and markedly higher than the third ($\Delta m \approx 4\%$ at 380–560 °C). The sample was stored in a dry atmosphere, and surface water loss (at $T \leqslant 100$ °C) was not detected. At 110 °C loss of crystal water occurs, with the formation of the anhydrous compound. At higher temperatures (200–380 °C) hydroxide groups condense, and at 380–560 °C the condensation of hydrogenphosphate groups takes place, giving the pyrophosphate α-TiP_2O_7. The DTA trace shows three endothermic peaks corresponding to stepwise dehydration and a first-order exothermic peak (*ca.* 750 °C, $\Delta m = 0$) associated with transformation of the pyrophosphate to its high-temperature (cubic) form.

Fig. 2(*a*) shows the X-ray powder diffraction (XRD) profile of Ti(OH)P. A low-angle peak typical of layered materials is present and is assigned to a layer spacing $d_{002} = 10.2$ Å. After heating the material overnight at 100 °C the XRD profile of the solid is unchanged (no dehydration has occurred), but treatment at 160 °C overnight leads to dehydration and moves the

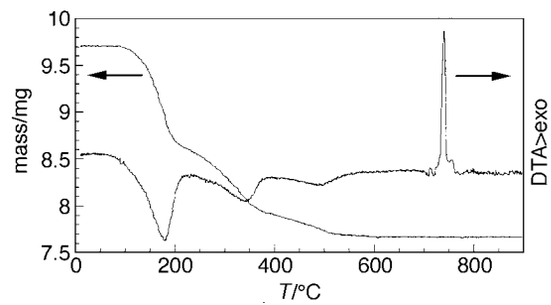

Fig. 1 The TG and DTA traces for Ti(OH)P

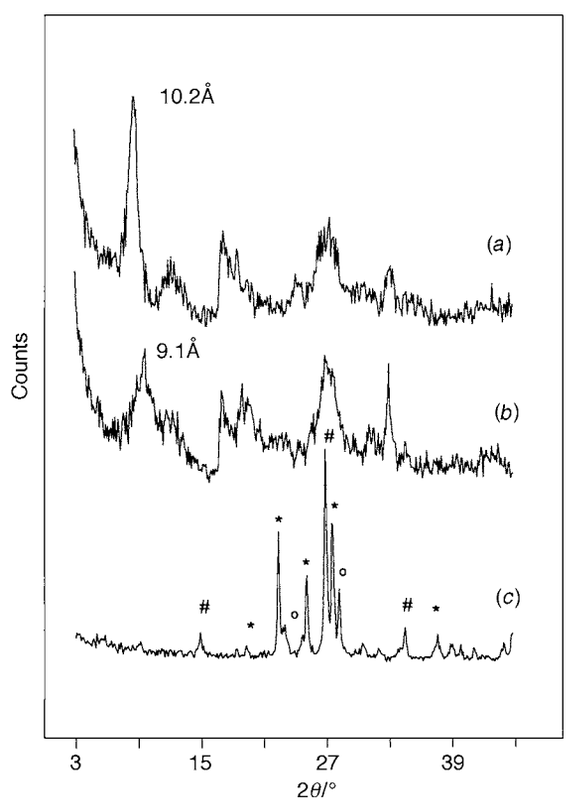

Fig. 2 The XRD profiles for (*a*) Ti(OH)P, and for solids obtained after treatment at (*b*) 160 and (*c*) 900 °C. Phases present are identified as follows: TiP_2O_7 (*), TiO_2 (rutile) (#) and $Ti_{10}O_{19}$ (○)

first diffraction peak to higher angle/lower *d* spacing [Fig. 2(*b*)]. The interlayer distance is then $d_{002} = 9.1$ Å, which might be associated with anhydrous β-TiP[13,14] (β-TiP is the anhydride

Table 1 Specific surface area for Ti(OH)P calculated by BET and t-plot methods as a function of the outgassing temperature, T

T/°C	25	100	160
S_{BET}/m² g^{-1}	86	91	90
C_{BET}	80	102	94
S_t/m² g^{-1}	87	92	89

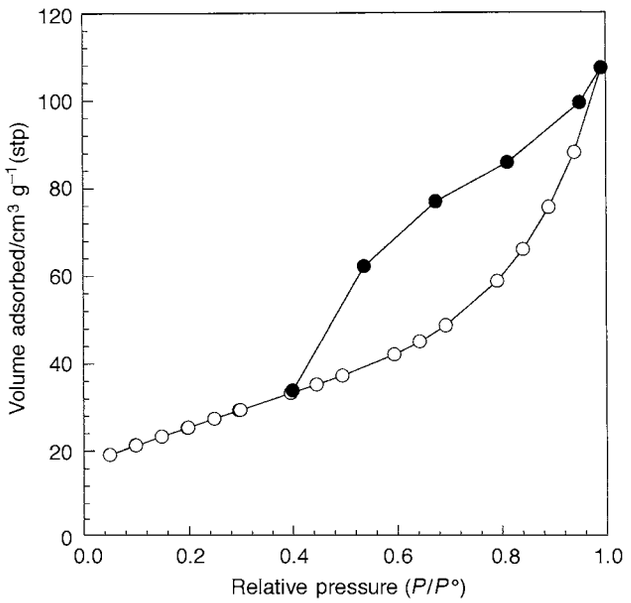

Fig. 3 Nitrogen adsorption–desorption isotherm of Ti(OH)P at 77 K (sample outgassed at 100 °C)

derived from γ-TiP). The strongest peak (d = 3.42 Å) for β-TiP is, however, not present in the XRD profile of dehydrated Ti(OH)P.

A sample of Ti(OH)P was calcined in air at 900 °C for 10 h. Such treatment of layered crystalline titanium phosphate phases (α- and γ-TiP) yields pure titanium pyrophosphate (TiP_2O_7). The XRD profile of calcined Ti(OH)P, however, also shows peaks associated with titanium oxides [Fig. 2(*c*)], as expected for a solid with P/Ti < 2.

Surface area and porosity

Fig. 3 shows the nitrogen adsorption–desorption isotherm (T = 77 K) for Ti(OH)P outgassed at 100 °C. Samples outgassed at different temperatures showed similar isotherms, which indicates that the surface area and porosity (texture) do not vary significantly during the thermal treatment. Dehydration during thermal treatment at 160 °C does not, therefore, affect the texture of the material.

The layer spacing in Ti(OH)P is $d_{002} \approx 10$ Å. Taking into account that the thickness of each layer is ≈5 Å (in most titanium phosphates), an interlayer gap of only 5 Å will be present. Isotherms of type IV of IUPAC classification,[15] with hysteresis loops of type H3, were found in this work. Such isotherms are characteristic of non-microporous solids, with porosity in the mesoporous range and resulting from defective layer stacking and voids between aggregated particles. The analysis of such isotherms is well established, and a discussion of the methods employed is presented by Gregg and Sing.[16]

Fig. 4 shows the t-plot (a comparison of the empirical isotherm to the standard isotherm[16]) typical of samples treated at 160 °C; a straight line at low relative pressures extrapolates to the coordinate origin, consistent with the absence of microporosity. Table 1 compares the values of specific surface area calculated from Brunauer–Emmett–Teller (BET) and t-plot methods, as well as the values of the C parameter in the BET

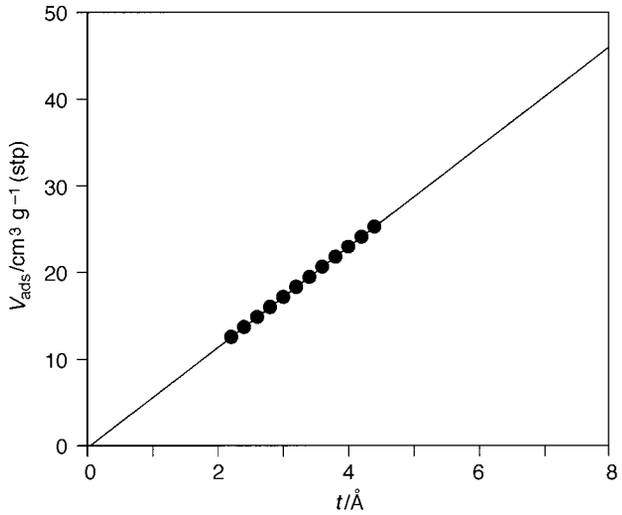

Fig. 4 The t-plot for Ti(OH)P treated at 100 °C

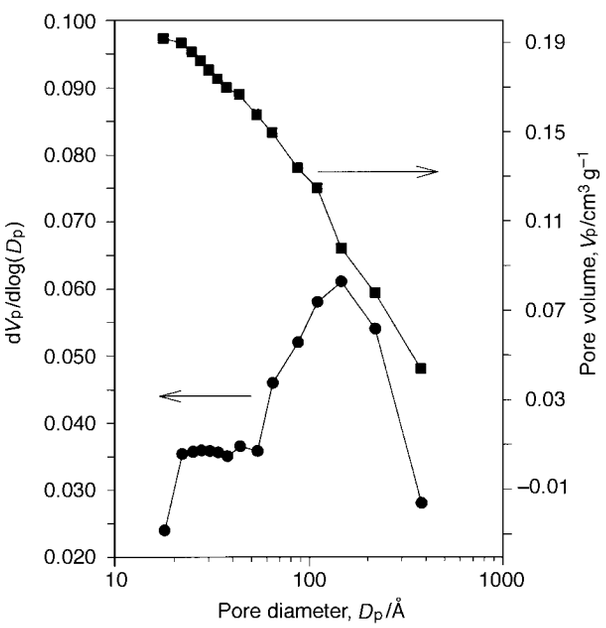

Fig. 5 Cumulative and differential pore volumes of the Ti(OH)P sample treated at 100 °C (cylindrical model)

model (the low C values reconfirm the absence of microporosity).

The pore-size distribution for a sample outgassed at 100 °C can be seen in Fig. 5. The distributions obtained from the adsorption and desorption branches are similar. Both present a maximum at a pore radius, R_p = 74 Å (pore diameter, D_p = 148 Å). The isotherm shape (with a hysteresis loop of type H3, Fig. 3), together with the strong increase in slope at $p/p^0 > 0.90$, suggest that the mesopores are full of liquid nitrogen at that pressure. The increasing adsorption at these higher pressures may be due either to the presence of some macroporosity or a swelling effect due to the nitrogen adsorption.

An adequate geometrical model for the analysis of the mesoporosity in this material is not easy to define. The lamellar nature of the atomic-level structure could suggest a porosity with slit shapes, but other factors suggest otherwise. The agreements between (*i*) the pore-volume distributions obtained from sorption and desorption branches, (*ii*) cumulative (Fig. 5) and adsorbed volumes and (*iii*) cumulative and BET surface areas indicate that the cylindrical pore model is the most appropriate in analysis of this mesopore distribution.

Table 2 Microanalytical data and experimental mass loss (TG) at 900 °C for the intercalation compounds, and those calculated from ideal formulae

	Experimental (%)			Calculated (%)		
Formula	C	N	Loss	C	N	Loss
$Ti(OH)_2(H_{0.5}PO_4)\cdot 0.5MeNH_3\cdot H_2O$	2.55	3.4	25.67	2.85	3.3	28.60
$Ti(OH)_2(H_{0.5}PO_4)\cdot 0.5C_2H_5NH_3\cdot H_2O$	5.6	3.25	27.27	5.5	3.2	30.90
$Ti(OH)_2(H_{0.5}PO_4)\cdot 0.5C_3H_7NH_3\cdot H_2O$	8.2	3.15	29.69	8.4	3.05	33.20
$Ti(OH)_2(PO_4)\cdot C_4H_9NH_3\cdot H_2O$	17.55	5.35	43.47	17.85	5.6	43.88
$Ti(OH)_2(PO_4)\cdot C_6H_{13}NH_3\cdot H_2O$	24.4	4.8	51.02	24.25	4.7	49.17
$Ti(OH)_2(PO_4)\cdot C_7H_{15}NH_3\cdot H_2O$	27.75	4.75	52.30	27.0	4.50	51.46
$Ti(OH)_2(PO_4)\cdot C_8H_{17}NH_3\cdot H_2O$	29.9	4.3	54.42	29.55	4.3	53.55

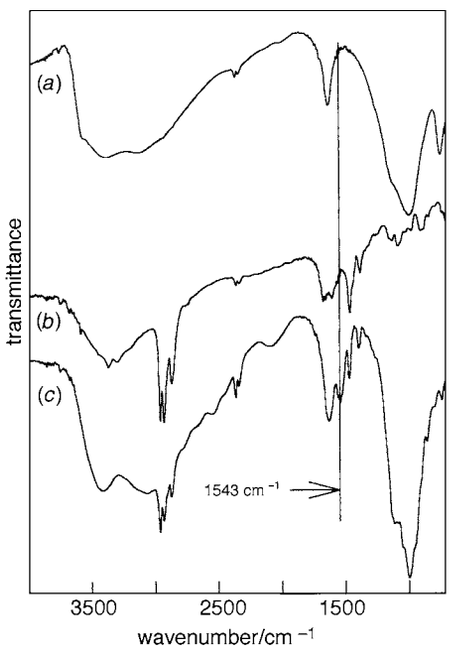

Fig. 6 Infrared spectra of (*a*) Ti(OH)P, (*b*) *n*-butylamine and (*c*) Ti(OH)P–*n*-butylamine intercalate

n-Alkylamine intercalation

The absorption of *n*-alkylamine vapours by layered phosphates gives rise to air-stable intercalation compounds. According to Casciola *et al.*[17] the intercalation of *n*-alkylamines in layered phosphates may be considered as an acid–base topotactic solid-state reaction between a solid acid host and a Brönsted-base guest. The intercalation process in Ti(OH)P may be represented by equation (1). The protonation of amines can be demon-

$$Ti(OH)_2(HPO_4)\cdot H_2O + RNH_2 \longrightarrow Ti(OH)_2(HPO_4)\cdot xRNH_2\cdot yH_2O \quad (1)$$

strated by applying spectroscopic techniques. Infrared spectra of the Ti(OH)P–*n*-butylamine intercalate and of the starting materials are compared in Fig. 6. That of the intercalate can be reproduced as the addition of those of Ti(OH)P and *n*-butylamine, but with an additional band at 1543 cm^{-1} attributed to protonated amine groups, NH_3^+.[18] The infrared spectra of all *n*-alkylamine intercalation compounds are similar, with the presence of NH_3^+ always being detected.

Intercalation of *n*-alkylamines into α-TiP is significantly different from that into γ-TiP, consequent upon the differing structural chemistries of the hosts. The cross-sectional area of a *trans-trans* alkyl chain is 18.6 $Å^2$.[19] If the free area for each acid centre is higher than that required by an amine molecule, steric factors do not prevent the material becoming saturated with adsorbate. The free area surrounding each phosphate group in α-TiP is 21.6 $Å^2$,[20] which permits the accommodation of one amine molecule (A) per phosphate (Ti : A = 1 : 2). A monolayer is obtained when only one POH group of every two is engaged in a bond with the amine groups. The arrangement of the guests in intercalation compounds with Ti : A < 1 : 1 leads to the formation of a bilayer since there is insufficient space for the interpenetration of alkyl chains of amines bound to phosphate groups of neighbouring layers. In contrast, the free area of the acid centre (16.4 $Å^2$)[21] in γ-TiP is lower than in α-TiP, and steric hindrance should be encountered due to interaction of amines associated with adjacent active centres. Obtaining Ti : A = 1 : 2 in γ-TiP is geometrically impossible.

In *n*-alkylamine intercalation of Ti(OH)P the rate of reaction decreases with increasing alkyl chain length. A product of low crystallinity is obtained after 6 h with methylamine, but only after 30 d with octylamine. The XRD profiles show two different behaviours in the intercalation of Ti(OH)P. (*i*) When methyl-, ethyl- or propyl-amine are intercalated lamellar materials of low crystallinity are obtained after a few contact hours, but their analyses (Table 2) are consistent with incomplete reaction. Furthermore, if these solids are left in the corresponding amine vapour, they transform into amorphous gels and the percentage of the amine in the solid increases. These amines lead to progressive destruction of the layer structure, as opposed to simple intercalation. (*ii*) The intercalation compounds formed with higher *n*-alkylamines (pentylamine up to octylamine) are, in contrast, more crystalline and retain that crystallinity independent of contact time. Their analyses (Table 2) are consistent with straightforward intercalation. Table 2 lists formulations for the products obtained, as deduced from elemental (C,N) microanalysis and TG. Short-chain *n*-alkylamines (methyl up to propyl) give a maximum molar ratio Ti : amine (A) of 1 : 0.5 for initial products, but higher amine contents were obtained for amorphous gels. For higher amines (pentyl up to octyl) the maximum Ti : A ratio obtained was 1 : 1; the intercalation process then involves all acid centres in Ti(OH)P, as in layered α-TiP.[22]

For those amines giving intercalation compounds (pentyl up to octyl) the variation in the layer spacing, d_{002}, of the intercalates with the length of the amine carbon chain (n_c) is consistent with the hypothesis that intercalation takes place with the formation of a double layer of amine molecules in *trans-trans* conformation almost perpendicular to the Ti(OH)P layer. Table 3 lists d_{002} values for the intercalates, along with literature data[21,22] for analogous compounds obtained with α- or γ-TiP as layered acid host. In this study d_{002} increases linearly with n_c (Fig. 7), following equation (2). The *n*-alkylamine intercalation

$$d_{002} = 12.5 + 2.20\, n_c \quad (2)$$

compounds of the α-MP family (M = Ti, Zr, Sn or Hf) show a similar behaviour.[23–25] As the length of an alkyl chain in *trans-trans* conformation increases by 1.27 Å for each additional carbon atom,[6] and as the slope of the straight line defining the interlayer distances is higher than 1.27 Å, the amine must be present in the Ti(OH)P as a bimolecular layer. The average inclination angle of the molecules with respect to the sheet is then $\alpha = \sin^{-1}(2.20/2.54) = 60.0°$. This angle is similar to that reported previously for the *n*-alkylamine arrangement in α-TiP

Table 3 Layer spacing, d_{002}/Å, for intercalated titanium phosphate hosts

Intercalated amine	α-TiP	γ-TiP	Ti(OH)P
Methylamine	13.1	13.5	13.0
Ethylamine	14.3	16.2	14.4
Propylamine	16.9	18.4	16.6
Butylamine	18.8	20.5	21.5
Hexylamine	23.1	24.6	25.5
Heptylamine	25.6	—	27.5
Octylamine	27.5	—	30.5

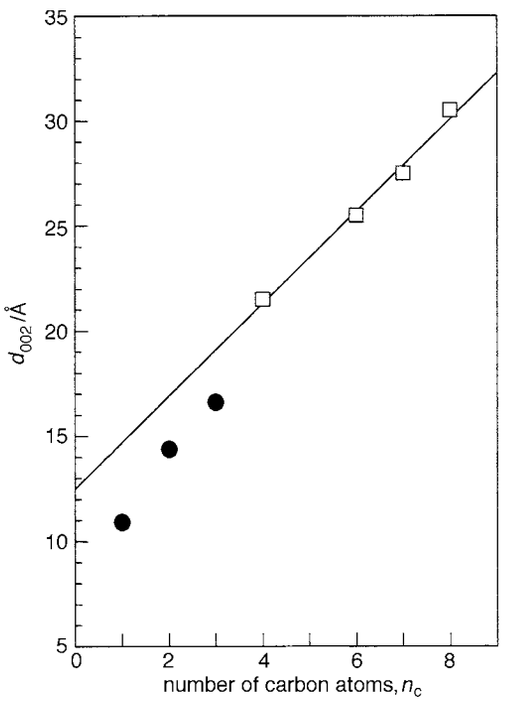

Fig. 7 Interlayer distance (d_{002}) of intercalation compounds of Ti(OH)P with *n*-alkylamines [containing 1 mol of amine per mol of titanium(IV)] as a function of the number of carbons, n_c, in the alkyl chain. □, Intercalation compounds of Ti(OH)P: ●, incomplete reaction and progressive gel formation from Ti(OH)P

(58.7°),[22] and lower than that obtained for intercalation in γ-TiP (64.9°).[21]

Ion-exchange capacity

With the presence of $HOPO_3$ (acid phosphate) groups in the structure of Ti(OH)P, this material should, by analogy with metal(IV) phosphates,[1–6] exhibit cation-exchange properties in neutral and alkaline media. Ion exchange in α phases takes place by diffusion of the cations from the surface of the solids towards the bulk, with an advancing phase boundary (two-phase behaviour). The γ phases show lower steric hindrance to the diffusion of cations and the process occurs preferentially with a continuous expansion of the interlayer region.[4]

The theoretical ion exchange capacity of Ti(OH)P (calculated from its formula) is 5.10 mequivalents g^{-1}. Studies on the ion-exchange capacity of this solid were performed using model solutions of alkali-metal ions. The adsorption of Na^+ and K^+ in Ti(OH)P was studied by using a potentiometric titration method. The exchange isotherms and the titration curves as a function of the MOH added are given in Fig. 8. The absolute values for the alkali-metal cation uptake *versus* model solution acidity are presented in Fig. 9. Addition of MOH to suspensions of Ti(OH)P should, initially, increase the pH of the solution. In the process of ion exchange a certain number of hydroxyl groups (equal to that of the sodium ions exchanged) will be neutralised. If the reaction behaves ideally

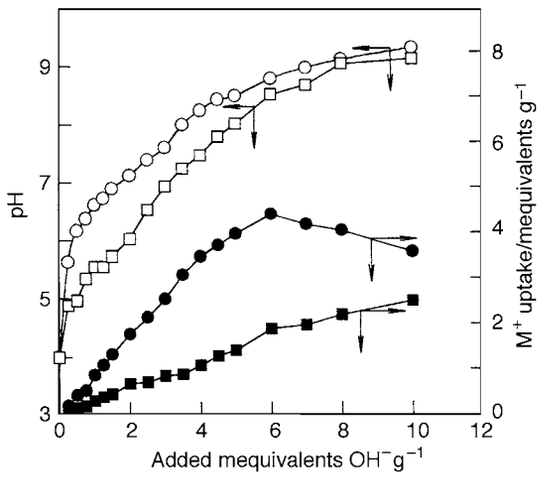

Fig. 8 Titration curves (○, Na^+; □, K^+) and ion-exchange isotherms (● Na^+; ■, K^+) for Ti(OH)P

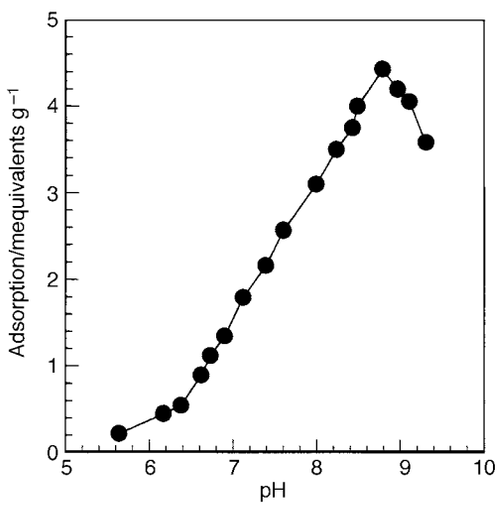

Fig. 9 Adsorption capacity as a function of equilibrium pH (potentiometric titration with NaOH) for Ti(OH)P

the equilibrium and initial pH values should be very similar. However, the analysis of M^+ ions in solution indicates that a greater number of hydroxyl groups has been used up than the quantity of Na^+ held by the exchanger. This is a result of hydrolysis reactions which, depending on the equilibrium pH, can take different forms. Analysis of the data in Fig. 9 shows alkali-metal uptake only at pH > 6, evident in a steep increase of slope in the adsorption curves at pH 6.5–7.0 for both alkali–metal cations. The potentiometric titration curves in Fig. 8 do not show any significant differences and have only one plateau (in the range pH 8–9), despite the large amount of alkali added.

In the Na^+–H^+ ionic substitution the layer spacing d_{002} (determined by XRD) in the solid was little different after exchange. In the K^+–H^+ system, however, a second phase with d_{002} = 11.2 Å was detected during progressive ion exchange. A continuous expansion of the layer spacing was not observed, and the ion-exchange behaviour is, therefore, similar to that shown by α-layered materials (as opposed to γ-layered materials).

Electrochemical studies: impedance spectra and conductivity

The conductivities of the acid phosphates and phosphonates of tetravalent metals are of contemporary interest.[4,26] All have in common that the conductivity is strongly dependent on relative humidity and that the host acts as a Brönsted acid toward the water of hydration, which is generally loosely bound in the structure. According to Alberti *et al.*[4] the conductivity of

Table 4 Arrhenius parameters for the a.c. conductivity of Ti(OH)P at different relative humidities

Relative humidity (%)	E_a/kJ mol^{-1}	$\log_{10}(A$/S K cm$^{-1})$
0	52	3.23
40	38	3.63
60	32	2.87
80	29	2.73
100	31	3.11

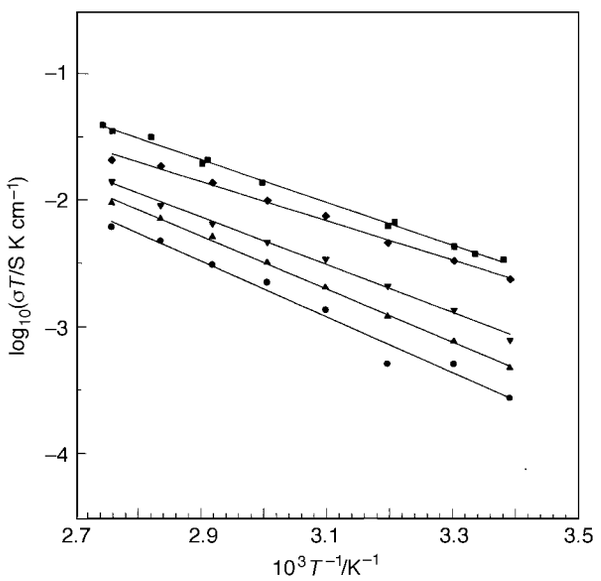

Fig. 10 Conductivity for Ti(OH)P as a function of temperature and of relative humidity [0 (●), 40 (▲), 60 (▼), 80 (◆), 100% (■)]

layered phosphates at near-ambient temperatures is dominated by surface transport. Proton NMR relaxation studies demonstrated the absence of any translational motion of protonic species through the bulk.[27]

The impedance plane plots obtained for Ti(OH)P samples consist of a single depressed semicircle (due to the bulk electrolyte resistance) with a low-frequency tail (due to electrode–pellet interfacial impedance). The sample resistance was determined by extrapolation of the high-frequency arc to the real axis, and converted into conductivity (σ) *via* sample geometry. In the temperature range 20–90 °C plots of $\log_{10}(\sigma T)$ *versus* $1/T$ are linear (Fig. 10) and can be interpreted by using an empirical Arrhenius-type equation [$\sigma T = A \exp(E_a/RT)$]. The E_a and A values are listed in Table 4 for 0–100% relative humidity. The activation energy increases with decreasing relative humidity (and level of hydration). At constant temperature, observed conductivities are some two to three orders of magnitude greater when measurements are carried out at 100 than at 0% relative humidity. Water molecules, therefore, play an important role in the conduction process. The conductivity is also seen to increase by two orders of magnitude when the temperature is increased [at 0% relative humidity, $\sigma_{(25\,°C)} = 9.7 \times 10^{-7}$ and $\sigma_{(90\,°C)} = 1.7 \times 10^{-5}$ S cm^{-1}; at 100%, $\sigma_{(25\,°C)} = 1.2 \times 10^{-5}$ and $\sigma_{(90\,°C)} = 1.1 \times 10^{-4}$ S cm^{-1}].

Attempts to improve the proton conductivity of layered phosphates and phosphonates by preparing new compounds with Brönsted bases intercalated in the interlayer region or in which functionalised organic radicals replace the hydroxyl of the phosphate groups have met some success.[28–30] The a.c. conductivity data for the *n*-alkylamine intercalates of Ti(OH)P are shown in Fig. 11 and Table 5. The conductivity values recorded for these intercalates are lower than that of the host material, as has been reported in layered phosphates (α and γ) for this family of guest molecules.[31] The low conductivity of the *n*-alkylamine intercalation compounds is a direct consequence of the basic strength of the guest molecule, the protons being localised on the amine groups (as shown by IR spectroscopy, Fig. 6).

Table 5 The a.c. conductivity at 25 °C and empirical activation energy (E_a) for Ti(OH)P and its *n*-alkylamine intercalates at 0% relative humidity

Compound	E_a/kJ mol^{-1}	σ/S cm^{-1}
$Ti(OH)_2(HPO_4)\cdot H_2O$	52	9.7×10^{-7}
$Ti(OH)_2(H_{0.5}PO_4)\cdot 0.5C_2H_5NH_3\cdot H_2O$	44	6.3×10^{-9}
$Ti(OH)_2(PO_4)\cdot C_4H_9NH_3\cdot H_2O$	44	6.6×10^{-9}
$Ti(OH)_2(PO_4)\cdot C_6H_{13}NH_3\cdot H_2O$	42	2.6×10^{-9}
$Ti(OH)_2(PO_4)\cdot C_7H_{15}NH_3\cdot H_2O$	37	1.0×10^{-9}
$Ti(OH)_2(PO_4)\cdot C_8H_{17}NH_3\cdot H_2O$	54	1.1×10^{-9}

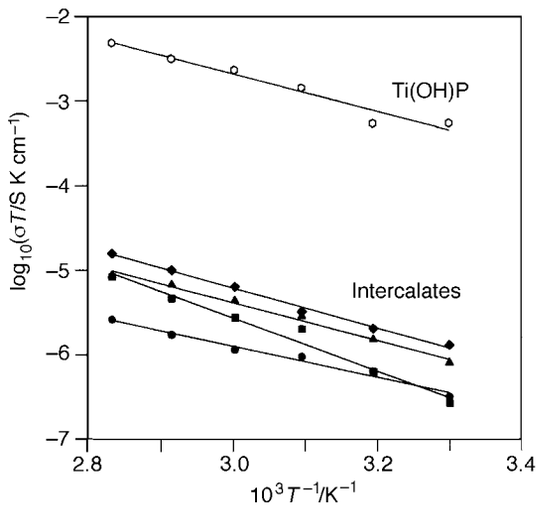

Fig 11 Arrhenius plots of conductivities of Ti(OH)P and its *n*-$CH_3(CH_2)_nNH_2$ intercalates [$n = 3$(◆), 5(▲), 6(●), 7(■) at 0% relative humidity]

Experimental

Synthesis

All reagents were of analytical grade (Aldrich) used without further purification. A solution of $TiCl_4$ (1 mol dm^{-3}, 80 cm^3) in HCl(aq) (2 mol dm^{-3}) was mixed with H_2O_2 (30% v/v, 10 cm^3) to obtain an intensely coloured titanium complex $[Ti(O_2)(OH)(H_2O)_x]^+$(aq). Phosphoric acid, H_3PO_4(aq) (1 mol dm^{-3}, 25 cm^3), was added. The resulting solution was refluxed at 60 °C in air for 6 d. The white precipitate obtained was filtered off and thoroughly washed with deionised water until the rinses had pH > 3. The solid was air dried at room temperature for 2 d, and then stored at room temperature under different relative humidities, controlled by H_2SO_4(aq) solutions of different densities (ρ = 1.00, 1.20, 1.30, 1.40 and 1.50 g cm^{-3} for 100, 80, 60, 40 and 20% relative humidity, respectively) or by $CaCl_2$(s) (0% relative humidity).

Instrumental

Thermal analyses (TG and DTA) were performed with a Stanton Redcroft STA-781 instrument (heating rate 10 °C min^{-1} in air). X-Ray powder diffraction (XRD) profiles were recorded with a modified Philips PW 1050 diffractometer and Ni-filtered Cu-Kα radiation (λ = 1.5418 Å). Infrared spectra were recorded on a Nicolet Magna 550 spectometer, using the KBr disc method. Sample surface area was investigated *via* adsorption–desorption isotherms (N_2 at 77 K) recorded using a Micromeritics Gemini instrument; the vapour pressure of the liquid-nitrogen bath was measured hourly and isotherms were

repeated to ensure reproducibility. Sample outgassing at 25, 100 or 160 °C was carried out for 5 h using a Micromeritics Flow-Prep 060.

Intercalation

Intercalation compounds containing *n*-alkylamines [$CH_3(CH_2)_nNH_3$, $0 \leqslant n \leqslant 7$] were obtained by placing Ti(OH)P (0.4 g) in an atmosphere saturated with the appropriate *n*-alkylamine vapour at room temperature for 1–60 d. The intercalated samples were air dried at 50 °C for 12 h, and stored in desiccators at different controlled relative humidities (as above).

Ion exchange

Adsorption of alkali-metal ions on Ti(OH)P employed model aqueous 0.05 mol dm^{-3} MCl–MOH (M = K or Na) solutions at $V:m = 200:1$ (cm^3:g) at room temperature. In all cases the contact time was 4 d and solutions were periodically shaken. The pH of the model solutions after equilibration with the adsorbent was measured using a Metrohm 713 pH meter. Residual concentrations of ions in solution [Na^+(aq), K^+(aq)] were measured using an atomic absorption spectrometer (Varian SpectraA 300).

Conductivity measurements

Electrical impedance measurements utilised a Solartron 1260 impedance analyser and 1270 electrochemical interface programmed *via* an IBM-compatible computer for data collection and analysis. Impedance spectra were recorded at 10 °C intervals in the range $20 \leqslant T/°C \leqslant 90$, using frequencies 5 Hz–13 MHz and an oscillating voltage of 300 mV. Pellets (13 mm diameter, 0.7–1.2 mm thick) were prepared by pressing 200 mg of material at 40 kN cm^{-2} in a pellet die. The two flat surfaces were painted with conductive silver paint (Electrodag 915, Acheson Colloids) to give ionically irreversible electrodes. The pellet was placed between two copper foils and the sample was spring loaded to ensure good electrode–electrolyte contact. The assembly was placed inside a cell maintained at controlled relative humidity by H_2SO_4(aq) or $CaCl_2$(s) (see above). The cell was allowed to equilibrate for at least 60 min at each temperature before measurements were taken (this time being found by experience to be much greater than the minimum necessary for temporal stability in impedance spectra). Experiments were repeated at least three times on different samples to ensure reproducibility, and average values are given.

Acknowledgements

We thank the Commission of the European Communities for funding this work under BRITE/EURAM II programme (contract BRE2-CT93–0535) and for a personal bursary for E. J. (contract BRE2-CT94–3096).

References

1 A. Clearfield, in *Inorganic Ion Exchange Materials*, ed. A. Clearfield, CRC Press, Boca Raton, FL, 1982, p. 1.
2 G. Alberti and U. Costantino, in *Inclusion Compounds*, eds. J. L. Atwood, J. E. D. Davies and D. D. MacNicol, Oxford University Press, Oxford, 1991, vol. 5, pp. 136–173.
3 A. Clearfield, *Chem. Rev.*, 1988, **88**, 125.
4 G. Alberti, M. Casciola, U. Costantino and R. Vivani, *Adv. Mater.*, 1996, **8**, 291.
5 G. Alberti, in *Recent Developments in Ion Exchange*, eds. P. A. Williams and M. J. Hudson, Elsevier Applied Science, London, 1987, p. 223.
6 J. R. García, R. Llavona, M. Suárez and J. Rodríguez, *Trends Inorg. Chem.*, 1993, **3**, 209.
7 P. Maireles-Torres, A. Jimenez-Lopez, P. Olveira-Pastor, I. Rodríguez-Ramos, A. Guerrero and J. L. García-Fierro, *J. Catal.*, 1992, **92**, 81.
8 D. Bianchi and M. Casciola, *Solid State Ionics*, 1985, **17**, 7.
9 G. Alberti, U. Costantino and M. L. L. Giovagnotti, *J. Inorg. Nucl. Chem.*, 1979, **41**, 643.
10 M. Suárez, J. R. García and J. Rodríguez, *Mater. Chem. Phys.*, 1983, **8**, 451.
11 Y. J. Li and M. S Whittingham, *Solid State Ionics.*, 1993, **63**, 391.
12 A. Bortun, E. Jaimez, J. R. García and J. Rodríguez, *Mater. Res. Bull.*, 1995, **30**, 413.
13 E. Kobayashi, *Bull. Chem. Soc. Jpn.*, 1975, **48**, 3114.
14 R. Llavona, J. R. García, M Suárez and J. Rodríguez, *Thermochim. Acta*, 1985, **86**, 81.
15 K. S. W. Sing, C. H. Everett, R. A. W. Haul, L. Moscou, R. A. Pierotti, J. Rouquerol and T. Simieniewska, *Pure Appl. Chem.*, 1985, **57**, 603.
16 S. J. Gregg and K. S. W. Sing, in *Adsorption, Surface Area and Porosity*, Academic Press, London 1982, chs. 2, 3.
17 M. Casciola, U. Costantino, L. di Croce and F. Marmottini, *J. Inclusion Phenom.*, 1988, **6**, 291.
18 L. J. Bellami, in *The Infrared Spectra of Complex Molecules*, Chapman & Hall, London, 1975.
19 A. I. Kitaigorodsky, in *Molecular Crystals and Molecules*, Academic Press, New York, 1973.
20 A. N. Christensen, E. K. Andersen, I. G. K. Andersen, G. Alberti, N. Nielsen and M. S. Lehmann, *Acta Chem. Scand.*, 1990, **44**, 865.
21 A. Menéndez, M. Bárcena, E. Jaimez, J. R. García and J. Rodríguez, *Chem. Mater.*, 1995, **5**, 1078.
22 F. Menéndez, A. Espina, C. Trobajo and J. Rodríguez, *Mater. Res. Bull.*, 1990, **25**, 1531.
23 R. M. Tindwa, D. K. Ellis, G. Z. Peng and A. Clearfield, *J. Chem. Soc., Faraday Trans. 1*, 1983, 545.
24 E. Rodríguez-Castellón, S. Bruque and A. Rodríguez-García, *J. Chem. Soc., Dalton Trans.*, 1985, 213.
25 M. L. Rodríguez, M. Súarez, J. R. García and J. Rodríguez, *Solid State Ionics*, 1993, **63,** 448.
26 K. D. Kreuer, *Chem. Mater.*, 1996, **8**, 610.
27 R. C. T. Slade, C. R. M. Forano, A. Peraio and G. Alberti, *Solid State Ionics*, 1993, **61**, 23.
28 M. Casciola, S. Chieli and U. Costantino, *Solid State Ionics*, 1991, **46**, 53.
29 G. Alberti, L. Boccali, M. Casciola, L. Massinelli and E. Montoneri, *Solid State Ionics*, 1996, **84**, 97.
30 E. W. Stein, A. Clearfield and M. A. Subramanian, *Solid State Ionics*, 1996, **83**, 113.
31 M. Casciola, U. Costantino and F. Marmottini, *Solid State Ionics*, 1989, **35**, 67.

Received 7*th November* 1996; *Paper* 6/07591F